Fusion of Multispectral And Full Polarimetric SAR Images In NSST Domain

Gh. S. El-Tawel *ghada_eltawel@ci.suez.edu.eg*
Computer Science Dept., Faculty of Computers and Informatics,
Suez Canal University,
Ismailia, Egypt

A. K. Helmy *akhelmy@narss.sci.eg*
Data Reception, Analysis and Receiving Station Affairs Division,
National Authority for Remote Sensing and Space Sciences, Cairo, Egypt

Abstract

Polarimetric SAR (POLSAR) and multispectral images provide different characteristics of the imaged objects. Multispectral provides information about surface material while POLSAR provides information about geometrical and physical properties of the objects. Merging both should resolve many of object recognition problems that exist when they are used separately. Through this paper, we propose a new scheme for image fusion of full polarization radar image (POLSAR) with multispectral optical satellite image (Egyptsat). The proposed scheme is based on Non-Subsampled Shearlet Transform (NSST) and multi-channel Pulse Coupled Neural Network (m-PCNN). We use NSST to decompose images into *low frequency* and *band-pass* sub-band coefficients. With respect to low frequency coefficients, a fusion rule is proposed based on local energy and dispersion index. In respect of *sub-band* coefficients, m-PCNN is used to guide how the fused *sub-band* coefficients are calculated using image textural information.

The proposed method is applied on three batches of Egyptsat (Red-Green-infra-red) and radarsat2 (C-band full-polarimetric HH-HV and VV-polarization) images. The batches are selected to react differently with different polarization. Visual assessment of the obtained fused image gives excellent information on clarity and delineation of different objects. Quantitative evaluations show the proposed method can superior the other data fusion methods.

Keywords: Multi-spectral Data Fusion, POLSAR, NSST, m-PCNN.

1. INTRODUCTION

Image fusion is a process of incorporating different images originating from different sources to create more reliable information than that from individual sources, and recently it has received great attention in the remote sensing field.

In the processing of optical images, many land cover types and surface materials are identical in their spectral characteristics. This leads to great difficulty in image segmentation, classification and feature extraction [1] [2]. Usually, Optical satellites use different sensors (visible, near infrared and shortwave infrared) to form images of the earth's surface. Different targets reflect and absorb in a different way at different wavelengths. Thus, their spectral signatures can characterize the targets.

Synthetic aperture radar (SAR) system hits the objects over the earth with a guided microwave [3], then the object either absorb or scatter these waves in all directions. Absorption or scattering of incident wave depends mainly on the physical characteristics of the object. The SAR system records only part of the scattered wave in the direction of the receiving antenna. Some SAR systems transmit and receive waves with different polarization (POLSAR). In this, the system

records the polarization of returned waves and measures both the intensity and phase of the backscattered waves. It mainly characterizes intrinsic structural and dielectric properties of the target [3].

Therefore, the imaging system for an optical satellite images and radar satellite signals are evidently different. The optical images are mainly characterized by spectral resolution, which is a measure of its ability to discriminate features in electromagnetic spectrum [4]. Polarimetric Radar images provide a tool to identify different features based on dielectric properties and surface roughness. Integration of spectral characteristics of an object, devised from multispectral images, and physical properties (and surface roughness) originated from Polarimetric SAR images will provide a great role in many remote sensing applications.

In this paper, we propose a new scheme for integrating Multispectral optical images (MS) and Multi-polarization POLSAR images. Non-Sampled Shearlet Transform (NSST) is used to decompose the input images into low and band-pass sub-bands. For low frequency coefficients, we introduce an adaptive weight fusion structure based on regional local energy and local image texture features. Different textural factors, gradient, entropy, and spatial frequency, are taken as multiple stimuli to Multi channel Pulse Coupled Neural Network (m-PCNN) to guide the fusion process of *band-pass* sub-bands. The rest of the paper is organized as follows: Section 2 and 3 discs in the short-term the theory of the NSST and m-PCNN. Section 3 demonstrates the main frame of the proposed scheme and pronounces the fusion algorithm. Experimental results and the evaluations are discussed in Section 4. We present the conclusions in the last section.

2. POLARIMETRIC SYNTACTIC APERTURE RADAR (POLSAR)

POLSAR images uses that fact that the status of the received scattered signal reflects the characteristics of the illuminated objects such as roughness and dielectric constants [5]. Accordingly the polarimetric images can be used efficiently to recognize these properties. The scattering matrix [S] is a kind of relation between the incident and scattered wave [5,6] and is being expressed by:

$$\begin{bmatrix} E_V^r \\ E_V^r \end{bmatrix} = [S] \begin{bmatrix} E_V^t \\ E_V^t \end{bmatrix} = \begin{bmatrix} S_{HH} & S_{HV} \\ S_{VH} & S_{VV} \end{bmatrix} \begin{bmatrix} E_V^t \\ E_V^t \end{bmatrix} \qquad (1)$$

Where $E_H^r, E_V^r, E_H^t, and\ E_V^t$ are the received and transmitted electric fields of corresponding polarizations respectively, and S_{mn} is the matrix elements and defined as:

$$S_{mn} = |S_{mn}| e^{\,i\varphi mn} \qquad (2)$$

The incident and scattered wave are a complex quantity (amplitude and phase) and usually expressed in polarization term (the direction of incident / received wave). Four different combinations of transmitted and received polarizations are listed below.

HH: horizontal transmission and reception.
HV: horizontal transmission and vertical reception.
VV: vertical transmission and vertical reception.
VH: vertical transmission and horizontal reception.

A SAR system used in this paper (RADARSAT-2) has a single antenna for both transmission and reception, the relation $S_{HV} = S_{VH}$ [7] holds for the rest of this paper.

From equation 2, the main parameters that characterized POLSAR data are the amplitudes ($|S_{HH}|$, $|S_{HV}|$, $|S_{VV}|$) and the phases (φ_{HV} and φ_{VV}). The phase values are not absolute values [7], it is a relative to a certain phase plan, generally HH-polarization element is chosen as a reference

phase. In this paper, we use the first three parameters, $|S_{HH}|$, $|S_{HV}|$, $|S_{VV}|$, to be fused with multispectral Egypt-sat data (see app-1).

3. THE NON-SUBSAMPLED SHEARLET TRANSFORM (NSST)

Multi-resolution analysis tools, Discrete Wavelet Transform (DWT), have been widely applied to image fusion [8, 9]. DWT are mainly depends on multi-scale geometric analysis, and has many advantages such as localization and direction. On the other hand, the wavelet transform suffers from imperfect directionality (directional selectivity is very limited and cannot get optimal detail information) moreover; it is not shift-invariant, result in degraded information and bad fusion output [10]. In order to get better signal representation researchers introduce new signal analysis tools and used extensively in image fusion, including: Curvelet [11], Ridgelet [12], Contourlet [10,13], and so on.

Easley et al. proposed Non-Subsampled Shearlet Transform (NSST) [14], which is the mixture of non-subsampled Laplacian pyramid transform and different shearing filters. NSST provides a multi-scale and multi-directional framework which decomposes into one low-frequency sub-band (signifies the approximation component of the source image) and a series of directional band pass sub-bands. NSST also satisfies the prerequisite of the shift-invariance property. So it can capture more further information on different directional sub bands than that of the wavelet transform and contourlet transform. The decomposition of shearlet is close to contourlet transform, but it has an advantage over contourlet transform that the number of directions in NSST for the shearing filter is non-limited.

Additionally, inverse contourlet requires inverting directional filter banks, instead of a summation of the shearing filter in case of inverse shearlet transform. Consequently the implementation of shearlet is more efficient computationally [14].

Through this work, we used NSST to decompose the input images into low and sub-bands coefficients, apply a fusion rule followed by the inverse of NSST to construct the fused image.

4. PULSE COUPLED NEURAL NETWORK

The Pulse Coupled Neural Network “PCNN” is a neural model with single layer architecture. To model an image with a PCNN, we consider the following: the input neurons represent image pixels, pixel’s information (e.g. Intensity or texture) are represented as an external stimulus received by each neuron and the relation between neighbored pixels is represented as internal stimuli fed to each neuron. In this model each neuron connects with its surrounded neighbors. PCNN uses an internal activation system to accumulate the stimuli until it surpasses a dynamic threshold, resulting in a pulse output. Images generated at different iterations indicate the fine details of the input image (edges and small objects). The PCNN model is fully described in [15, 16].

Many researchers use PCNN for data fusion for instant Wang and Ma design single PCNN for medical image fusion [17, 18]. Miao introduces an adaptive system for image fusion with different spatial resolution by the adaptive linking coefficient of PCNN [19]. Others integrate PCNN with multi-layer decomposition to get the fused image [20, 21].

Recently a parallel version of PCNN is introduced in which many PCNNs are working in parallel, in this each network operates on a separate channel of the input [17]. We present an image fusion method based on dual pulse couple neural network [22]. Wang presented an excellent review of application of PCNN [23].

Our proposed scheme of data fusion is based on m-PCNN that is a modified version of PCNN. This model is proposed by Wang and Ma, [17, 18]. m-PCNN can extend the number of inputs that depends on practical request. We use some texture information as multiple stimuli of m-PCNN, and the output is used as a weight guide for the fusion process.

5. GENERAL FRAMEWORK OF MULTISPECTRAL-POLSAR FUSION ALGORITHM

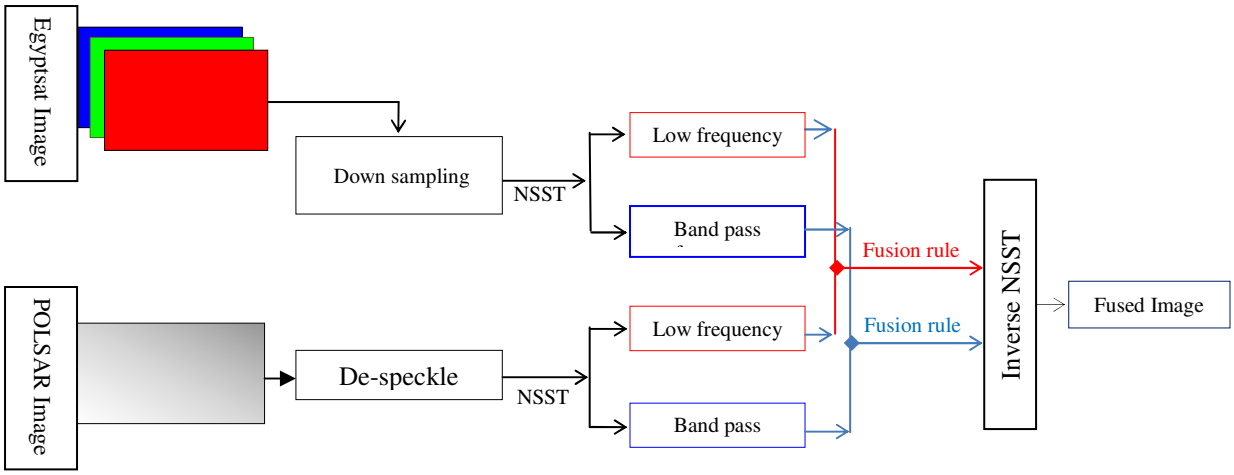

FIGURE 1: Block diagram of image fusion based on the NSST.

Through this paper, we assume that Egyptsat, and POLSAR images have been co-registered, and noted by R (x, y), M (x, y) respectively. F (x, y) is the output fused image. Figure-1 demonstrates the proposed framework of the image fusion process. As a summary, the fusion approach is listed in the following steps.

1- POLSAR image has been de-speckled and the Egyptsat image is down-sampled (from 7.8 to 7 meters) to match the POLSAR spatial resolution.
2- *Low frequency* and *band-pass* sub-bands coefficients of the source images are calculated using NSST.
3- The *low-frequency* sub-band coefficients and the directional *band-pass* sub-bands coefficients of the source images are merged according to specific rules, the rules will be introduced in the next sections.
4- Calculate the inverse NSST to get the fused image F (x, y).

5.1 Fusion Rule for Lowpass Coefficients

As the *lowpass* sub-band coefficients mainly retain the main energy and represent the approximation component of the source images, fusion procedures should be adopted to preserve this information. Many authors process the *lowpass* sub-band coefficients use direct averaging rule [24], which is simple, however, this scheme always results in a low-contrast effect, due to fact that both information (3-bands) of POLSAR and multispectral images are complementary and both of them are desirable in a fused image. A new average weighted formula has been presented to model fusion hierarchy based on regional local energy and local image texture features.

It is difficult to know or even estimate, which bands from POLSAR and multispectral should be fused together (in our case we have three-bands for multispectral image and three-bands represent POLSAR image). Figure 2 shows a schematic diagram of our method to fuse *lowpass* coefficients, and the procedures are summarized as follows:

1- For all bands, the local energy (equation-5) is calculated for each coefficient, using its neighborhood (5 x 5 in our case). This is done for the multispectral and POLSAR bands.

2- Coefficient retains maximum value of energy from POLSAR is fused with a coefficient that has the least energy from multispectral (equation-3). This represents the first-band first-fused coefficient.
3- To get the second-band first-fused coefficient, next coefficient with maximum energy from POLSAR is fused with preceding minimum energy from multispectral coefficient.
4- Finally, to get the third one, coefficient with minimum energy from POLSAR is fused with maximum energy from multispectral images. The mathematical notation of the process calculations is described below.

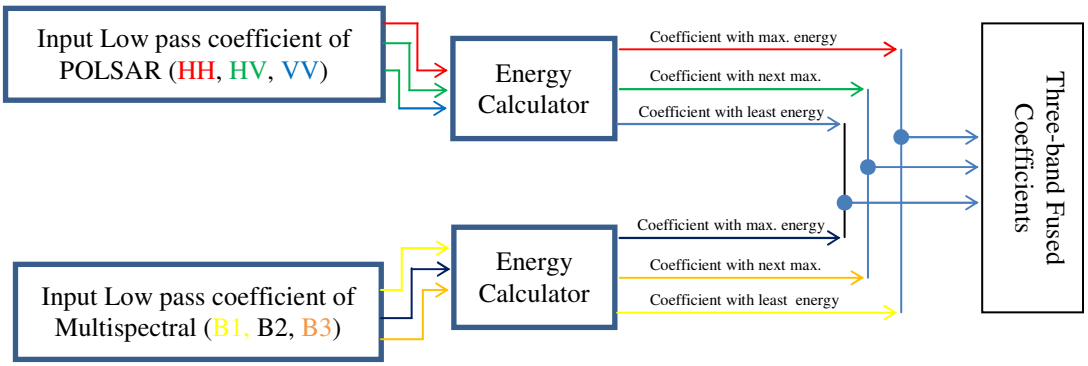

FIGURE 2: Block Diagram of Image Fusion rules for Low Coefficients.

The coefficient of the fused image at location (x, y) can be calculated by:

$$I_F\,(x,y) = \frac{w_1\, I_R(x,y) + w_2 I_M(x,y)}{2} \qquad (3)$$

Where:
$I_R(x,y), I_M(x,y)$, and $I_F(x,y)$ denote the lowpass *subband* coefficient located at(x,y) for POLSAR, multispectral and fused images respectively.

The value of $I_R(x,y)$ is chosen among the coefficients of three POLSAR bands according to the following:

$$I_R(x,y) = C(maximum\ (en_{hh}, en_{hv}, en_{vv})) \qquad (4)$$

Where: C (…) is the *lowpass suband* coefficients.

$en_{xx}(energy)$ is a parameter used to measure the textural uniformity of an image, $hh, hv\ or\ vv$, and calculated as follows:

$$en\,(x,y) = \frac{1}{n \text{ x } n} \sum_{m=-(n-1)/2}^{m=(n-1)/2} \sum_{r=-\frac{n-1}{2}}^{r=\frac{n-1}{2}} C^2(x+m, y+r) \qquad (5)$$

Where *C* is the *lowpass* coefficients of *HH, HV or VH*, and *n* and *m* are those defined the neighborhood areas.

In contrast the value of $I_M(x,y)$ is picked from the coefficients of three multispectral bands according to the following: $I_M(x,y) = C(minimum\,(en_{b1}, en_{b2}, en_{b3})\,)$, again *C (…)* is the *lowpass suband* coefficients.

The weights in the equation (3) can be calculated as follows:

$$w_1 = \frac{maximum\ (en_{hh}, en_{hv}, en_{vv})}{minimum\ (en_{b1}, en_{b2}, en_{b3})} \qquad (6)$$

$$w_2 = \frac{1}{w_1} \qquad (7)$$

In this $if\ w_1 > 1$: *i.e.)* maximum energy picked from POLSAR image is greater than the minimum energy of multispectral image, the proposed weighting strategy leads to maximize the contribution of POLSAR image and minimize that of multispectral image.

On the other hand $if\ w_1 < 1$ *i.e.)* minimum energy picked from multispectral image is greater than the maximum energy of POLSAR image, again our strategy leads to maximize the contribution of multispectral image and minimize that in POLSAR image. The previous procedures are repeated with next maximum and minimum values to obtain 3-bands fused image.

In any case, the high-energy contribution is maximized, while the minimum energy contribution minimizes through generation of the fused image. This procedure can overcome the low contrast drawback of weighting average scheme.

To fine-tune the results of fused coefficients and to obtain better effect than that explained earlier, we modified equations (6, 7) taking into account texture information when calculating the weight factor. We added a dispersion index "D" which is a normalized degree of dispersion of a probability distribution: it is a measure used to enumerate whether a set of observed occurrences is clustered or dispersed with respect to a standard statistical model. It is defined as the ratio of the variance "δ^2" to mean "μ" and calculated as an average mean for both images.

$$D = \frac{\delta^2}{\mu} \qquad (8)$$

Then the new weight

$$\widehat{w}_1 = w_1 + \frac{D_S}{D_m} \qquad (9)$$

Where $D_S\ and\ D_m$ are dispersion index of POLSAR and multispectral images.

5.2 Fusion Rule for High Frequency Sub-band Coefficients

The image edges, corners and other fine details are concentrated in the high-frequency components obtained from shearlet transform. Thus, the clarity and distortion of the fused image depend mainly on how these components are fused. Voting strategy has been popularly applied to composite the high-frequency components. It relies on constructing decision map using different parameters to regulate where the fused coefficients are from image 'A' or image 'B'.

In most existing fusion algorithms, usually, some textural information is used to decide from which the fused image come from [25]. Features such as the entropy, gradient, variance, and the spatial frequency [26, 27] can represent image texture information. Essentially, it can reflect detailed information in different ways, and can be used to discriminate sharp and indistinct regions. These textural measurements can be used independently [26, 27] or may be joint using some specific rules [28]. In our method, we present some texture information (the entropy, gradient and spatial frequency) as an indicator of weighting factor in constructing a fusion rule. These different texture factors are taken as multiple stimuli of m-PCNN. Then the output determines the fusion weight according to the values coming from PCNN that reflect the overall image clarity. The whole process shown in figure 3 and can be summarized as follows:

For the current subband, let $C_I^{l,k}(x,y)$ be the band-pass coefficient at a location (x,y) in the l^{th} band at k^{th} level, I represents HH, HV, VV, b1, b2 or b3.

For the same subband, calculate the maximum gradient($GR_{\max}$), entropy ($EN_{\max}$), and spatial frequency ($Sf_{\max}$) values among all bands.

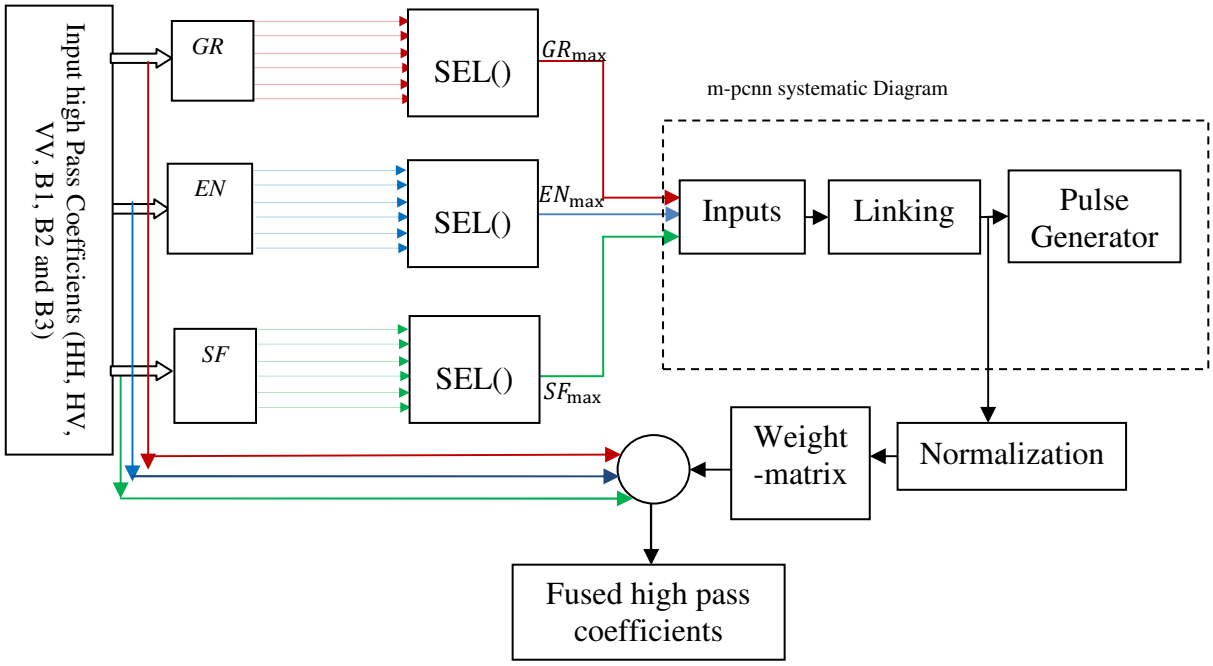

FIGURE 3: Block diagram of image fusion for subbands coefficients.

$$GR_{\max} = maximum\ (\ GR(C_I^{l,k}(x,y))\quad \forall(I) \qquad (10)$$

$$EN_{\max} = maximum\ (\ EN(C_I^{l,k}(x,y))\quad \forall(I) \qquad (11)$$

$$SF_{\max} = maximum\ (\ SF(C_I^{l,k}(x,y))\quad \forall(I) \qquad (12)$$

Where: $GR(C_I^{l,k}(x,y))$ is the gradient of the *high-pass* coefficient at location (x,y) in the l^{th} subband at k^{th} level. Similarly $EN(C_I^{l,k}(x,y))\ and\ sf(C_I^{l,k}(x,y))$ are the largest value of entropy and spatial frequency respectively of the *high-pass* coefficients.

Maximum gradient, entropy, and spatial frequency will be used as different features of image to motivate dual-channel m-PCNN. The fusion will be done between the three winner bands (bands that have maximum gradient, entropy and spatial frequency). We should keep track which bands got those maxima. The coefficient of the fused image at location (x, y) can be calculated by:

$$CI_F\ (x,y) = \frac{w}{3}\sum_{p=1}^{3} I_p\ (x,y) \qquad (13)$$

Where:
$I_p(x,y)$ Denote the high-pass *subband* coefficient located at(x,y) with a maximum value of gradient, entropy, and spatial frequency. W is the weight factor outputs from m-PCNN.

5.3 Assessment Criteria

The visual contrast between the fused images and original images are conducted. Furthermore, quantitative analysis is also applied to the results of different fusion algorithms in terms of correlation coefficients, entropy, average gradient [29] and the $Q^{AB/F}$[30]. The clarifications of these measures are discussed below.

The *correlation* reflects the amount of similarity of two images. The average gradient mirrors the difference between image structure (sharper image normally has a greater average gradient), the entropy specifies the overall randomness level in the image (higher value of entropy, more detailed information will be contained in the image), While $Q^{AB/F}$ measures the amount of edge information transferred from the source images to the fused image using a Sobel edge detector, its larger value, imply better fusion result is.

In the two images f(x,y) and B(x,y) of size M x N, the correlation coefficient of each band is defined as:

$$Correlaton\ coefficient = \frac{\sum_{\forall x}\sum_{\forall y}[(f(x,y) - E_A) \times (B(x,y) - E_B)]}{\sqrt{\sum_{\forall x}\sum_{\forall y}\left[(f(x,y) - (E_f)^2\right] \times \sum_{\forall x}\sum_{\forall y}\left[(B(x,y) - (E_B)^2\right]}} \quad (14)$$

Where E_f and E_B are the mean of two images, respectively.

$$average\ gradient = \frac{1}{(M-1)(N-1)}\sum_{\forall M}\sum_{\forall N}\sqrt{\frac{1}{2}\left[\left(\frac{\partial(f(x,y)}{\partial x}\right)^2 + \left(\frac{\partial(f(x,y)_2}{\partial y}\right)\right]} \quad (15)$$

$$entropy = -\sum_{\forall l} p(l)\ln p(l) \quad (16)$$

Where $p(l)$ means the probability of the gray value (l) appearing in the image.

$$Q^{AB/F} = \frac{\sum_{n-1}^{N}\sum_{m-1}^{M}(Q^{AF}(n,m)W^A(n,m) + Q^{BF}(n,m)W^B(n,m))}{\sum_{n-1}^{N}\sum_{m-1}^{M}(W^A(n,m) + W^B(n,m))} \quad (17)$$

Where $Q^{AF}(n,m) = Q_g^{AF}(n,m)Q_\alpha^{AF}(n,m)$; $Q_g^{AF}(n,m)$ and $Q_\alpha^{AF}(n,m)$ are the edge strength and orientation preservation values respectively; n, m represent the image location; and N ,M are the size of images. $Q^{BF}(n, m)$ is similar to $Q^{AF}(n, m)$. $W^A(n,m)$ and $W^B(n,m)$ reflect the importance of $Q^{AF}(n, m)$ and $Q^{BF}(n, m)$,respectively. The dynamic range of $Q^{\frac{AB}{F}}$ is [0 1], and it should be as close to 1 as possible.

6. EXPERIMENTAL RESULTS

Data fusion algorithms in literatures take advantage of the complementary spatial/spectral resolution characteristics of multi-spectral and panchromatic data for producing spatially enhanced multi-spectral observations. In our instance, spatial resolution is almost the same while the complementary information resides in spectral bands. We seek to integrate information from Red, Green and infrared bands (exist in Egyptsat images) with other information originated from POLSAR data that represent geometric and physical characteristics of objects

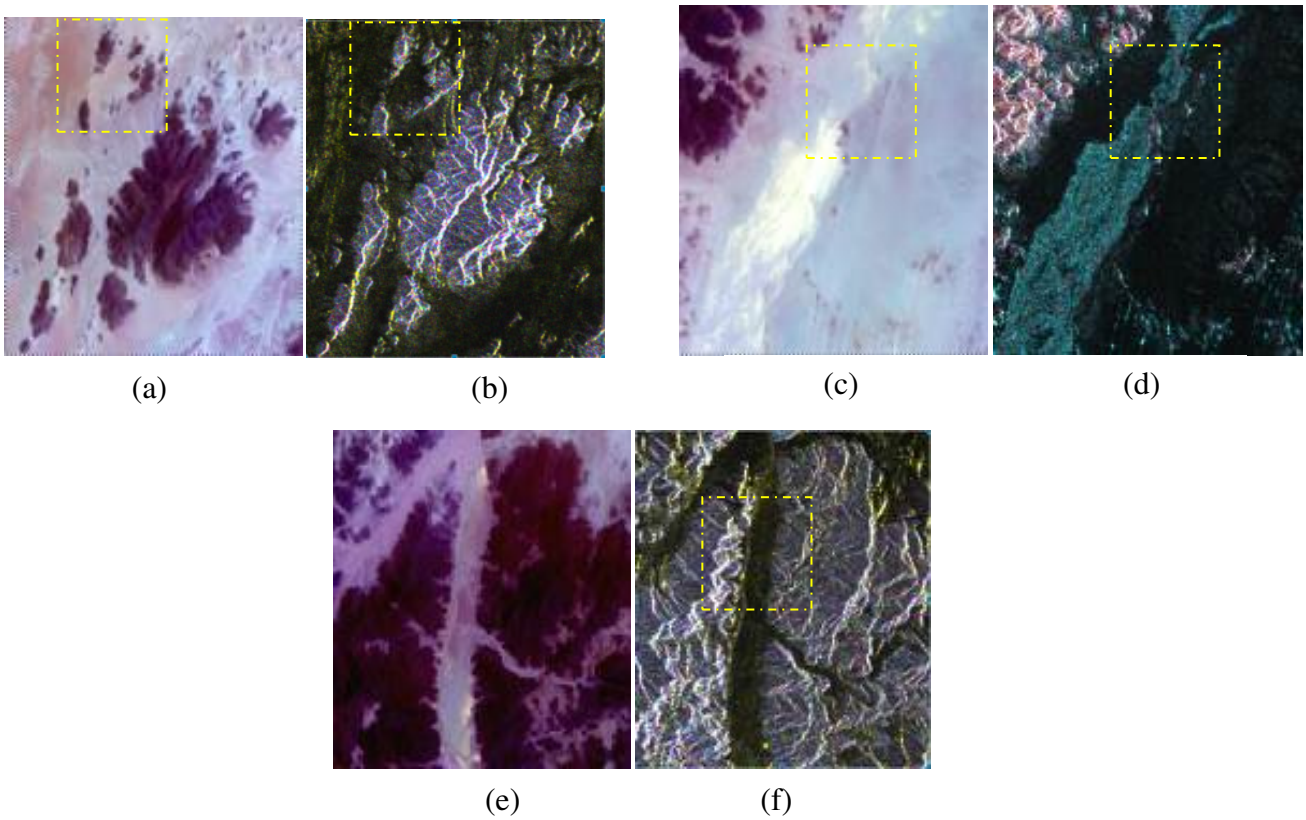

FIGURE 4: Three Input batches a-b-c: Multispectral images (in RGB color composite). b,d,f: C-band raw polarimetric SAR image (R=HH,G=HV,B=VV), *copyright (MDA)*

The proposed scheme is used to merge multispectral, Egyptsat, image (Band 1, Band 2 and Band 3-see-App1), with scattering matrix of POLSAR with *HH, HV and VH* polarization taking into account that *HV=VH*. The POLSAR data set used is C-band Radarsat-2 (RS-2) data in a full parametric mode. Spatial resolution of POLSAR is 7 m; while Egyptsat is 7.8 m., Speckles of POLSAR are reduced using enhanced LEE filter [31], while the spatial resolution of Egypt sat is down-sampled to match that of POLSAR. The data set has been accurately co-registered. To illuminate the results, three batches (pat-1, pat-2 and pat-3) of images are used as shown in figure 4. The batches are carefully chosen to be sensitive to radar-objects interaction (i.e. vertical and horizontal polarized). Comparing the proposed scheme with traditional methods [32] used in remote sensing such as principal component, brovey, IHS… is not appropriate in our case, since these techniques aim to merge multispectral with PAN SAR images.

In order to evaluate the proposed method we had made a comparison with three fusion methods, SIST-based [33], PCNN-based [22], and Contourlet-based [13]. In these methods, the fusion process is performed separately with respect to S_{HH} ,S_{HV} and S_{VV} , then the fused results are displayed in RGB. Moreover, the proposed scheme is compared with that proposed by Lei Wang that has the ability to fuse two multispectral images [34]; he used Hidden Markov Tree (HMT) in SIST domain to perform fusion process.

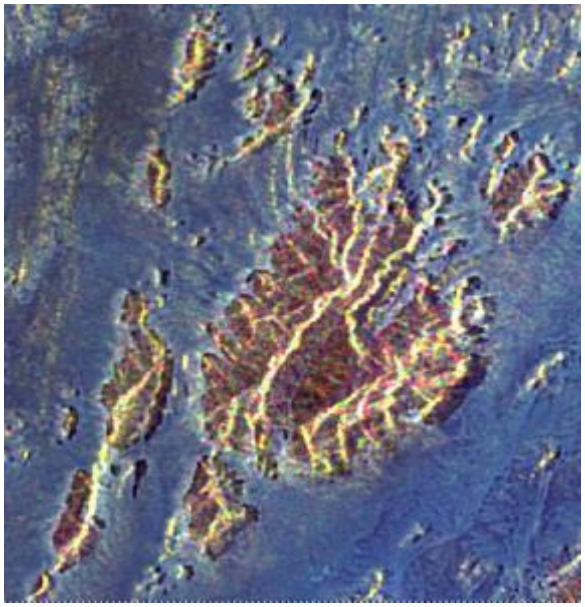

(a)

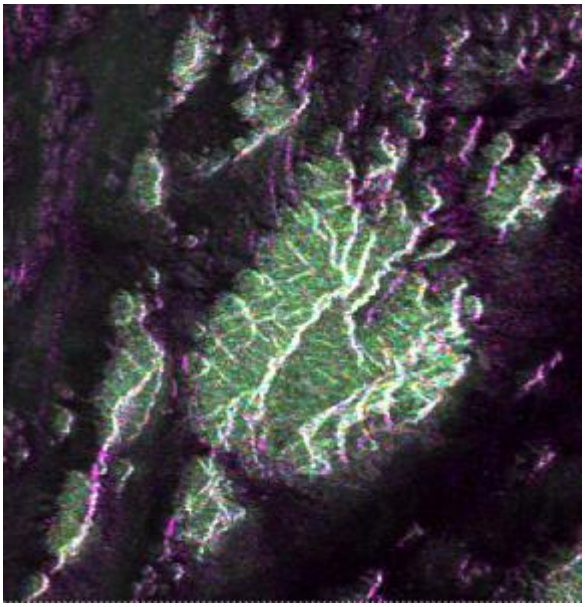

(b)

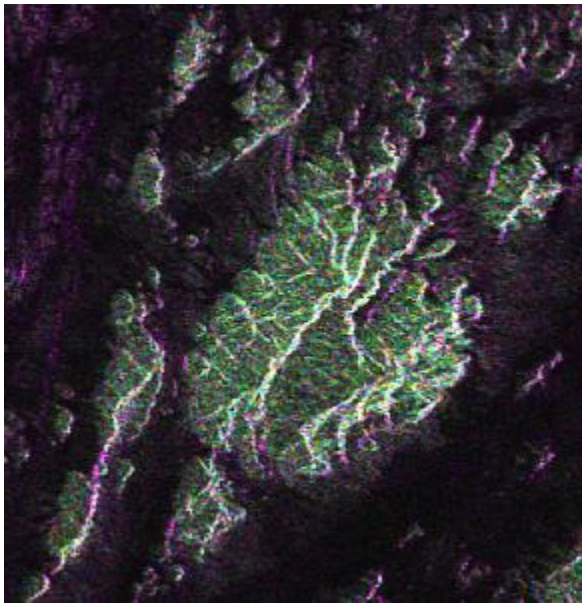

(c)

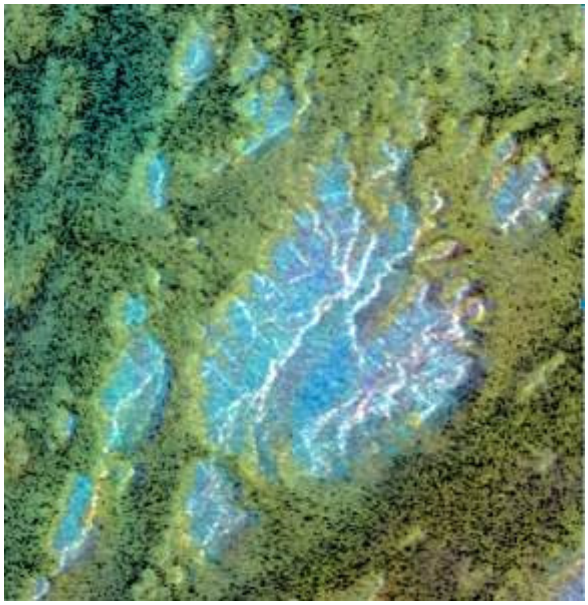

(d)

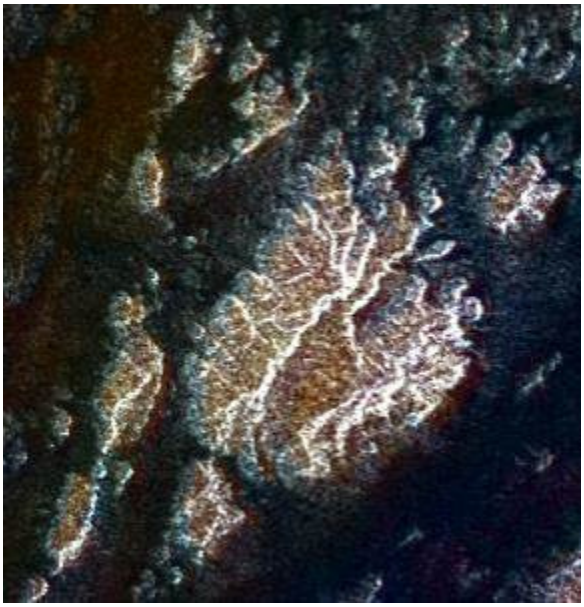

(e)

FIGURE 5: The fusion results: of Fig. 4 (a) and (b): (a)–(e) fused images using the proposed method, SIST-based, Contourlet-based, HMT-based and PCNN-based, respectively.

Figure 4 shows the source images used in this research. We use three batches of images in the fusion experiment; the images are selected to react differently with different POLSAR polarization. One group focuses on a hilly area, second emphasis flat region and the last one contain both of them. Figure 5 shows the fusion results of batch-1. Generally, although all methods inject fair information of the source images into the fused image, but they fail to achieve acceptable transfer of information, specifically that related to low frequency regions, from input images to the fused image. To clarify the visual assessment, figure 6 shows closer look of these images.

Closer looks at these results disclose the following:

As can be seen in figures 5 and 6, the fused image, which is obtained by HMT-based, presents low contrast and vague attendance; Moreover, it showed a loss of edge information and mixing of color in low frequency sub-bands, this due to only use of intensity component in the fusion process [34].

The fused image, SIST-based Method, lost information to some extent in low frequency subbands. In addition, edges suffer from over smoothness.

The fused images outs from Contourlet-based appear noticeable noise at high frequency regions (the edges), as it does not have shift-invariant, which leads humble visual effects.

PCNN method shows an improvement in visual effects, although it suffers from overall haziness appearance. The proposed methods introduced significant migration of information from input images to the fused one in both low and sub-bands frequency.

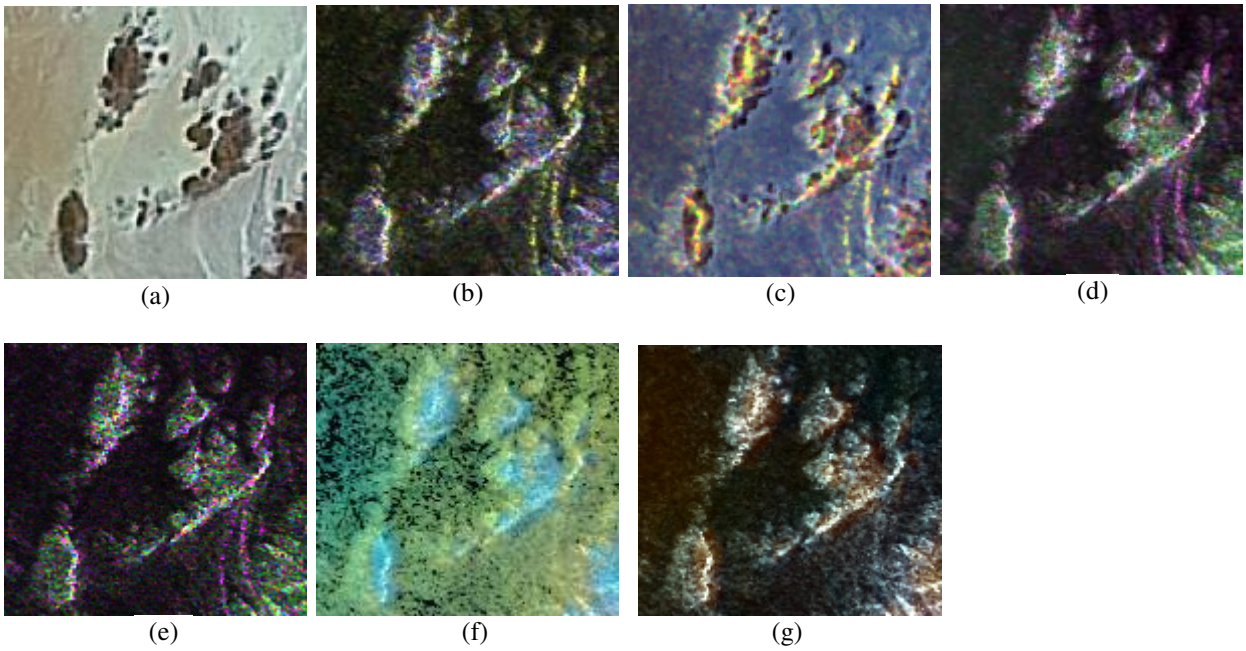

FIGURE 6: Zoomed shot of the fusion results: (a) and (b): Multispectral and POLSAR input images. (c)– (g): zoomed area of fused images using the proposed method, NSST-based, Contourlet-based, HMT-based and PCNN-based respectively.

TABLE 1: Comparison of fusion results with different fusion methods (batch-1, the radar image is sensitive to vertical polarization, it is a steep region)

	Proposed Model	SIST-Based	Contourlet-Based	HMT-Based	PCNN-Based
Correlation	0.88	0.85	0.83	0.8	0.83
Average-gradient	8.644	8.1	8.8	7.8	8.4
Entropy	8.457	8.2	8.5	7.38	8.1
$Q^{AB/F}$	0.792	0.77	0.73	0.61	0.69

According to the quantitative evaluation, table-1 lists different metric measures used through this study, best values achieved by the proposed model regarding the amount of information, transferred from input images to the output, and the strength of the edges. Zoomed areas of the second and third batches of the image are shown in figures 7, 8. Tables 2, 3 show the quantitative measures of fused images.

TABLE 2: Comparison of fusion results with different fusion methods (batch-2, the radar image is sensitive to horizontal polarization, it is almost flat region).

	Proposed Model	SIST-based	Contourlet - Based	HMT-Based	PCNN-Based
Correlation	0.88	0.81	0.78	0.7	0.785
Average-gradient	6.192	6.1	5.87	5.4	5.7
Entropy	7.069	7	7.1	6.5	6.9
$Q^{AB/F}$	0.75	0.7	0.66	0.711	0.74

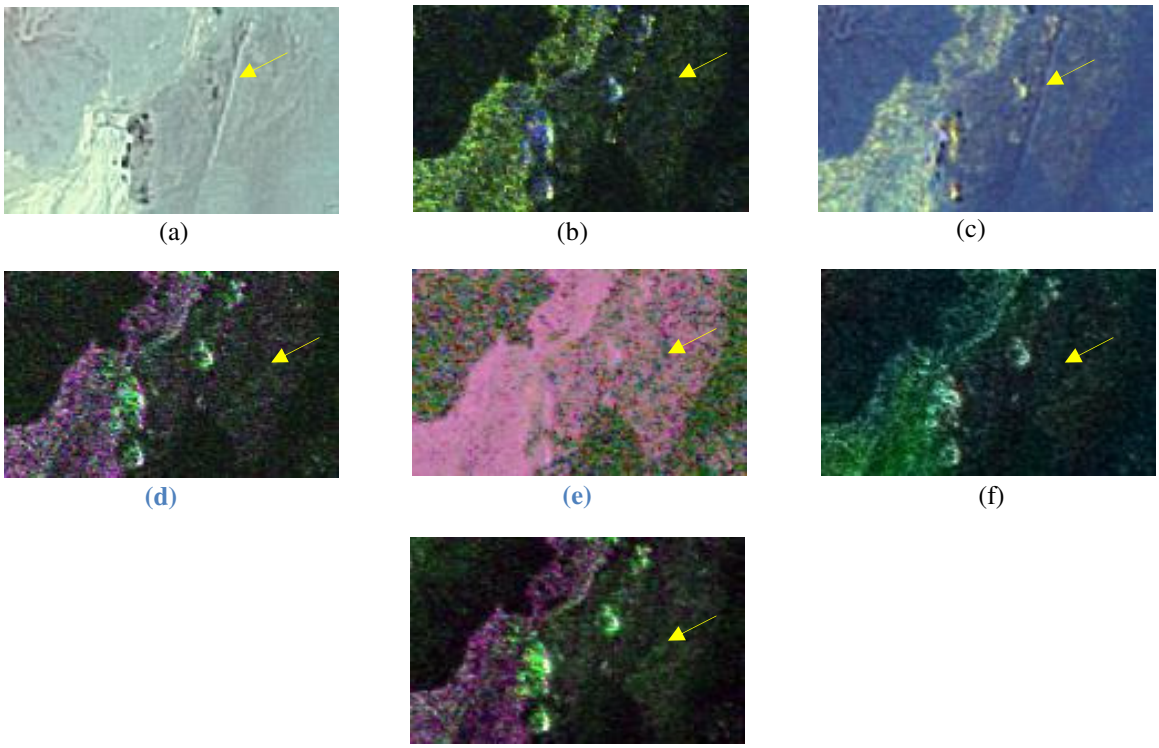

FIGURE 7: Zoomed area of the second batch of images: (a) and (b): Multispectral and POLSAR input images. (c)– (g): fused images using the proposed method, NSST-based, Contourlet-based, HMT-based and PCNN-based respectively.

Figure 7, 8 give same indication, some high frequency components eliminated from fusion results; it was pointed by the yellow arrow in figure 7. In Figure 8, it is found that the valley structures are fully preserved in the proposed method, while the color information is variegated between multispectral and POLSAR images.

TABLE 3: Comparison of fusion results with different fusion methods (batch-3, the radar image is sensitive to both horizontal and vertical polarization).

	Proposed Model	**SIST**	**Contourlet - Based**	**HMT-Based**	**PCNN-Based**
Correlation	0.91	0.91	0.88	0.73	0.86
Average-gradient	7.2	6.87	6.99	7.04	5.9
Entropy	8.15	7.59	8.1	7.9	6.5
$\mathbf{Q^{AB/F}}$	0.68	0.679	0.523	0.61	0.59

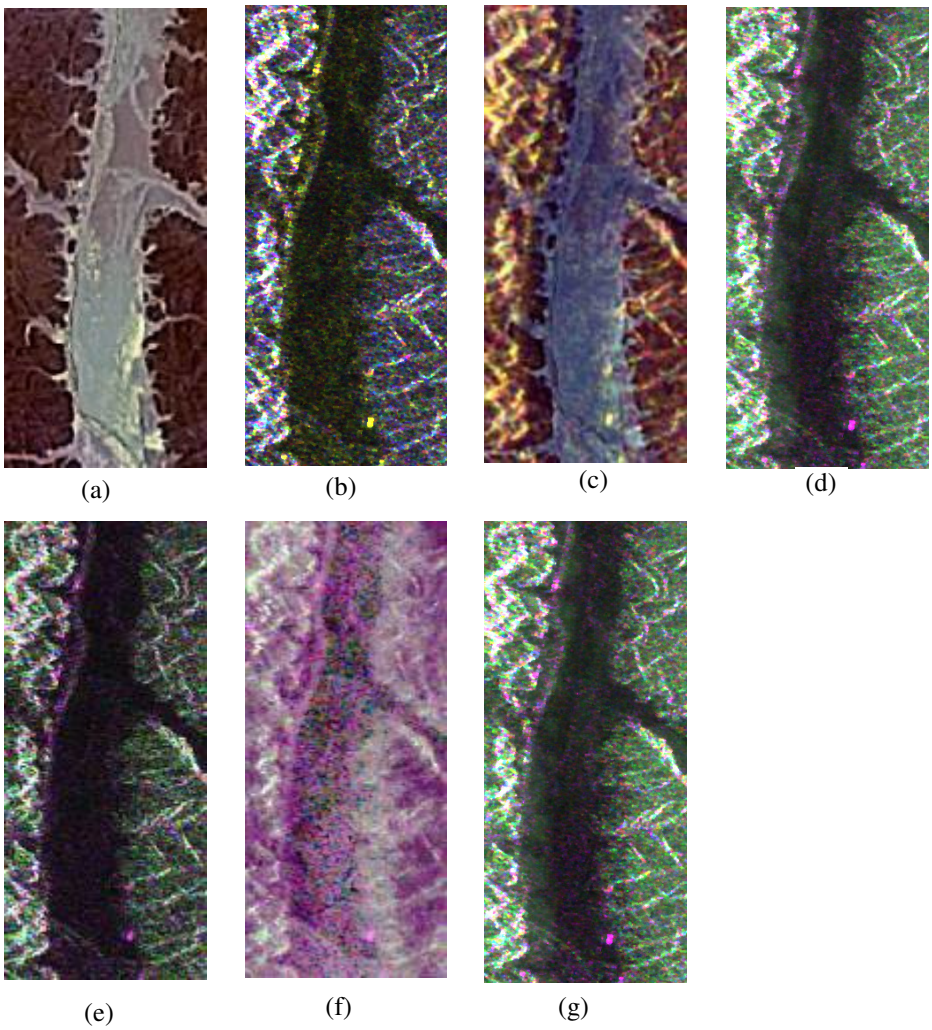

FIGURE 8: Zoomed area of the third batch of images: (a) and (b): Multispectral and POLSAR input images. (c)– (g): fused images using the proposed method, NSST-based, Contourlet-based, HMT-based and PCNN-based respectively.

7. CONCLUSION

This research investigates the fusion process of full polarimetric POSAR data, RS2, with Multispectral optical imagery (Egyptsat). By applying the fusion process, we obtain a new image that can be considered neither optical nor POLSAR. It is a synthesized image that is produced for better image understanding. To meet this requirement, we propose a new weighting average scheme based on NSST and m-PCNN. Firstly, input images are transformed into *low* and band-pass sub-bands. Low frequencies of both images are fused to each other by relating maximum and minimum energy of both images-bands with a reciprocal way, in addition, the fusion process takes into account a texture distribution by adding a dispersion index to the fused coefficients. Secondly, m-PCNN is used to guide the fusion process of band-pass sub-bands by incorporating edge information measurements. The experimental results indicate that the fused image has strengthened object structure detail.

ACKNOWLEDGMENTS

We express our deepest thanks and appreciation to the Canadian Space Agency (CSA) for providing the Radar Sat 2 images for this study under the agreement of the project ID5128. We also acknowledge the National Authority for Remote Sensing and Space Sciences for resourcing this work.

8. REFERENCES

[1] King, RL. 2000. "A challenge for high spatial, spectral, and temporal resolution data fusion" In: Proceedings, IEEE international geoscience and remote sensing symposium, IGARSS no. 6: 2602–2604. doi: 10.1109/IGARSS.2000.859654.

[2] Zhu, X., and Yin L. 2001. "Data fusion of multi-sensor for petroleum geological exploration" In: Proceedings, international conferences on infotech. and info-net, ICII, Beijing no.1: 70–75. doi: 10.1109/ICII.2001.982723.

[3] Sabry R., and Vachon P. W. 2014. "A Unified Framework for General Compact and Quad Polarimetric SAR Data and Imagery Analysis." IEEE Transactions on Geoscience and Remote Sensing 52(1): 582-602. doi:10.1109/TGRS.2013.2242479.

[4] Campbell, J. B. 2002. Introduction to Remote Sensing, New York London: The Guilford Press.

[5] Giorgio, L. 2014. "A novel approach to polarimetric SAR data processing based on Nonlinear PCA" Pattern Recognition no. 47:1953–1967. doi: 10.1016/j.patcog.2013.11.009.

[6] Kajimoto, M. 2013. "Urban density estimation frompolarimetric SAR images based on a POA correction method" IEEE Journal of Selected Topics in Applied Earth Observations and Remote Sensing 6(3): 1418–1429. doi: 10.1109/JSTARS.2013.2255584.

[7] Jong-Sen, Lee, and Eric Pottier. 2009. Polarimetric Radar Imaging: From Basics to Applications. CRCPress: BocaRaton.

[8] Huang, W., and Jing Z.L. 2003. "Evaluation of focus measures in multi-focus image fusion" Pattern Recognition Letter no. 28: 493–500. doi: 10.1016/j.patrec.2006.09.005.

[9] Shutao, Li., and Bin Yang. 2008. "Multi-focus image fusion using region segmentation and spatial frequency" Image and Vision Computing no. 26: 971–979. doi: 10.1016/j.imavis.2007.10.012.

[10] Zhang, Q., and Guo, B.L. 2009. "Multifocus fusion using the non subsampled contourlet transform" Signal Processing 89(7): 1334–1346. doi: 10.1016/j.sigpro.2009.01.012.

[11] Starck, J.L., Candes, E.J., and Donoho, D.L. 2002. "The curvelet transform for image denoising" IEEE Transaction on Image Processing 11(6): 131–141. doi: 10.1109/TIP.2002.1014998.

[12] Candes, E. 1998. "Ridgelets: Theory and Applications", Technical report, Department of Statistics, Stan-ford University, https://statistics.stanford.edu/sites/default/files/1998-17.pdf.

[13] Huafeng Li., Chai, Yi., and Zhaofei Li. 2013. "Multi-focus image fusion based on nonsubsampled contourlet transform and focused regions detection" Optik - International Journal for Light and Electron Optics 124(1): 40–51. doi: 10.1016/j.ijleo.2011.11.088.

[14] Easley, G., Labate, D., and Lim, W.Q. 2008. “Sparse directional image representations using the discrete shearlet transform” Applied and Computational Harmonic Analysis 25 (1): 25–46. doi: 10.1016/j.acha.2007.09.003.

[15] Ranganath , H. S. and Kuntimad, G., 1999. “Object Detection Using Pulse Coupled Neural Networks” IEEE Transactions on Neural Networks 10, (3): 615–620. doi: 045-9227(99)03181-1.

[16] John L. Johnson and Mary Lou Padgett. 1999. “PCNN Models and Applications” IEEE Transactions on Neural Networks. 10(3): 480- 498. doi: 1045-9227(99)03191-4.

[17] Wang, Z., and Yide, Ma. 2008. “Medical image fusion using m-PCNN” Information Fusion 9 (2): 176– 185. doi: 10.1016/j.inffus.2007.04.003.

[18] Wang, Z., and Yide. Ma. 2007 “Dual-channel PCNN and its application in the field of image fusion” Proc. of the 3rd International Conference on Natural Computation no. (1):755–759. doi: 10.1109/ICNC.2007.338.

[19] Miao, Q. and Wang, B. 2005. “A novel algorithm of multi-focus image fusion using adaptive PCNN”, "A novel adaptive multi-focus image fusion algorithm based on PCNN and sharpness" Proc. SPIE 5778, Sensors, and Command, Control, Communications, and Intelligence (C3I) Technologies for Homeland Security and Homeland Defense IV, (704): doi:10.1117/12.603092.

[20] Xu, B., and Chen, Z. 2004. “A multisensor image fusion algorithm based on PCNN” Proc. of the 5th World Congress on Intelligent Control and Automation no. (4): 3679–3682. doi: 10.1109/WCICA.2004.1343284.

[21] Li, W. and Zhu, X. 2005. “A new image fusion algorithm based on wavelet packet analysis and PCNN”, Proc. of the 4th International Conference on Machine Learning and Cybernetics no. 9: pp. 5297–5301. doi: 10.1109/ICMLC.2005.1527879.

[22] El-taweel, Ghada Sami and Helmy, Ashraf Khaled. 2013. “Image fusion scheme based on modified dual pulse coupled neural network”, IET Image Processing 7(5): 407–414, doi: 10.1049/iet-ipr.2013.0045.

[23] Zhaobin Wang, Yide Ma , Feiyan Cheng, Lizhen. 2010. “Yang Review of pulse-coupled neural networks” Image and Vision Computing no. 28: 5–13, doi:10.1016/j.imavis.2009.06.007.

[24] Wang, Zhao-hui, Wang Jia-qi, Zhao De-gong, and Wei FU. 2012. “Image fusion based on shearlet and improved PCNN” Laser Infrared. 42(2): 213–216. http://caod.oriprobe.com/order.htm?id=29200739&ftext=base.

[25] Xuan Liu, Yue Zhou, and Jiajun Wang. 2014. “Image fusion based on shearlet transform and regional features” Int Journal Electronics and Communications (AEÜ) 68(6): 471-477. doi:10.1016/j.aeue.2013.12.003.

[26] Jingbo Zhang, et. al., 2008 . “Multi-focus image fusion using quality assessment of spatial domain and genetic algorithm” Conference on Human System Interactions 8(2): 71– 75. doi: 10.1109/HSI.2008.4581411.

[27] Liu, Wei, YIN Ming, LUAN Jing, and Guo Yu. 2013. “Adaptive image fusion algorithm based on Shift-invariant shearlet transform” Acta Photonica Sinica 42(4): 496-503. doi: 10.3788/gzxb20134204.0496.

[28] Lei, Wang, and Bin Li. 2012. "Multi-modal medical image fusion using the inter-scale and intra-scale dependencies between image shift-invariant shearlet coefficients" Information Fusion no. 19: 20-28. doi: /10.1016/j.inffus.2012.03.002.

[29] Wang, Z., Bovik, A.C., Sheikh, H.R., and Simoncelli, E.P. 2004. "Image quality assessment: from error visibility to structural similarity", IEEE Transaction on Image Processing 13 (4): 600–612. doi: 10.1109/TIP.2003.819861.

[30] Petrovic, V., and Xydeas, C. 2000. "On the effects of sensor noise in pixel-level image fusion performance" Proc. of the Third International Conference on Image Fusion no. 2: 14–19. doi: 10.1109/IFIC.2000.859842.

[31] Lee, J.S., Grunes, M. R. and Grandi, G. De. 1999. "Polarimetric SAR Speckle Filtering and its Implication for Classification", IEEE Transaction on Geoscience and Remote Sensing 37(5): 2363-2373. doi: 10.1109/36.789635.

[32] Jixian, Zhang. 2010. "Multi-source remote sensing data fusion: status and trends" International Journal of Image and Data Fusion 1(1): 5-24, doi: 10.1080/19479830903561035.

[33] Liu X, et al., .2014. "Image fusion based on shearlet transform and regional features". International Journal of Electronics Communications (AEÜ) 68(6): 471-477. doi:10.1016/j.aeue.2013.12.003.

[34] Lei Wang, and Tian Lian-fang. 2014. "Multi-modal medical image fusion using the inter-scale and intra-scale dependencies between image shift-invariant shearlet coefficients" Information Fusion no. (19): 20-28. doi:10.1016/j.inffus.2012.03.002.

Appendix 1. The spectral resolutions of the Egyptsat-1 data

Bands	Description	Wavelength (μm)	Resolution (m)
Band 1	Green	0.51-0.59	7.80
Band 2	Red	0.61-0.68	7.80
Band 3	Near infrared	0.80-0.89	7.80
Band 4	Panchromatic	0.50-0.89	7.80
Band 5	Mid infrared	1.10-1.70	39.5